

Article

Thermomechanical Characterization of SiC/SiC Ceramic Matrix Composites in a Combustion Facility

Ragav P. Panakarajupally ^{1,*}, Michael J. Presby ¹, K. Manigandan ¹, Jianyu Zhou ², George G. Chase ² and Gregory N. Morscher ¹

¹ Department of Mechanical Engineering, The University of Akron, Akron, OH 44325, USA; mjp80@zips.uakron.edu (M.J.P.); mk77@zips.uakron.edu (K.M.); gm33@uakron.edu (G.N.M.)

² Department of Chemical Engineering, The University of Akron, Akron, OH 44325, USA; jz61@zips.uakron.edu (J.Z.); gchase@uakron.edu (G.G.C.)

* Correspondence: rp95@zips.uakron.edu

Received: 29 April 2019; Accepted: 6 June 2019; Published: 17 June 2019



Abstract: A combustion facility which includes uniaxial mechanical loading was implemented that enables environmental conditions more akin to jet engine environments compared to conventional static environment tests. Two types of woven SiC/SiC ceramic matrix composites (CMCs), melt-infiltrated (MI) and chemical vapor infiltrated (CVI), were subjected to fatigue loading in the combustion facility and under isothermal furnace conditions. Some CVI test coupons were coated with a multilayer environmental barrier coating (EBC) of mullite + ytterbium monosilicate using slurry infiltration process to demonstrate the performance with a coating. Combustion conditions were applied using a high velocity oxy fuel gun on the front side of the specimen and mechanical loading was applied using a horizontal hydraulic MTS machine. All the specimens considered were subjected to tension-tension fatigue loading at 100 MPa, stress ratio of 0.1 and specimen front-side surface temperature of 1200 ± 20 °C. Nondestructive evaluation (NDE) methods, such as electrical resistance (ER), was used as an in-situ health monitoring technique. Similar fatigue tests were performed in an isothermal furnace for comparison. A much lower fatigue life was observed for the uncoated specimens tested under combustion conditions in comparison to isothermal furnace condition. This difference in fatigue life was attributed to damage associated with added thermal stress due to the thermal gradient and higher rate of oxidative embrittlement due to the presence of high velocity combustion gases in the combustion environment. EBC coating increased the fatigue life in combustion environment. However, EBC coated specimens experienced spallation in the high-velocity flame due to the presence of micro cracks in the coating surface. Fracture surfaces of the failed specimens were investigated under the scanning electron microscope (SEM) to determine the extent of oxidation and damage.

Keywords: burner rig; fatigue characterization; ebc coating; electrical resistance; high temperature

1. Introduction

Ceramic matrix composites (CMCs) are candidate materials for future propulsion components because of their high temperature capability, reduced cooling requirements, low weight, and high specific strength. An increase in turbine inlet temperature with advanced cooling and homogenous combustion increases the efficiency of the jet engine and decreases the NO_x emissions [1]. Current nickel-based superalloys employed in jet engines are operating at their maximum operating temperatures with advanced cooling and protective thermal barrier coatings and cannot withstand any increase in temperature. Silicon carbide (SiC) fibers embedded in SiC matrix have the ability to withstand high temperatures [2]. At high temperatures, SiC ceramics resist oxidation by forming a protective oxide

layer of SiO₂. In a water vapor-containing combustion environment, SiO₂ volatilizes to Si(OH)₄, leading to material recession and a significantly reduced life of the component [3,4]. The application of EBC coating can protect the material from surface recession, and hence, increase the life of the material. Numerous studies [5,6] have investigated whether the durability and failure of different EBC coatings indicate the increased life of the component over several hundreds of hours in oxidizing environments. However, in jet engine combustion conditions, coating cracks and spallation of the coating can occur, which provides a free path for the combustion gases to enter into the system posing a threat to the substrate material [7].

Successful implementation of CMCs in jet engines requires characterizing these materials in environments approaching jet engine conditions. This involves a combined mechanical loading and combustion environment. Several studies have been conducted to understand the material behavior at high temperatures [8–10]. However, these studies were performed in laboratory conditions using an isothermal furnace, which is incapable of simulating combustion environment. In recent years, very few studies were performed to characterize the CMCs in jet engine environments using burner rig facilities [11–13]. These studies showed a decreased fatigue life in burner rig environment compared to furnace conditions due to rapid oxidation and material recession because of the presence of high water vapor content and thermal gradient stress.

The high velocity of the combustion gases present in the burner rig environment can be detrimental on the life of the composite. For example, Ogbuji [14] reported that burner rig specimens (velocity of 100 m/s) with 10% water vapor content suffered more severe strength degradation than the furnace specimens with 90% water vapor at 800 °C. He attributed this to the high velocity of the flame, which is adequate to push the oxidizing gases deep into the core of the composite, leading to large recession of a thin carbon layer between the fibers and the BN interphase which is not observed in the furnace conditions. The conclusion was that the high-velocity flame in the burner rig depletes the carbon layer along the length of the fibers at a much faster rate than the BN layer, exposing the BN, which in turn forms a borosilicate liquid cladding the fibers.

The change in electrical resistance (ER) is an established method to monitor the damage in carbon fiber composites [15]. Recent studies on CMCs demonstrated ER as a successful in-situ method to monitor the damage progression at room and high temperature, as ER is very sensitive to temperature and damage [16,17]. Therefore, to understand the mechanical behavior and to monitor the damage of the materials closer to jet engine conditions, a unique experimental facility was developed along with incorporating health-monitoring techniques, which can simulate various mechanical and combustion conditions of advanced aircraft engines.

The main objective of this study is an initial investigation toward understanding the effect of combustion environment on the mechanical properties and damage mechanisms of coated and uncoated melt-infiltrated (MI) and chemical vapor infiltrated (CVI) specimens. ER was used as an in-situ health-monitoring technique to monitor the damage. Fracture surfaces were investigated under scanning electron microscope (SEM) for the extent of oxidation. A comparison between the effects of isothermal and combustion conditions are discussed.

2. Experimental Procedure

2.1. Burner Rig Facility

To produce the combustion environments, a unique burner rig facility is developed which can simulate coupled thermomechanical loading. A high-velocity oxygen fuel (HVOF) gun (HP 2700 HVOF system, Plasma Powders & Systems, NJ, USA) is used to simulate the jet engine combustion environment while the mechanical loading is applied using a horizontal hydraulic MTS machine (MTS 810 system). The HVOF gun uses propane and oxygen as fuel and oxidizer to create a high-temperature, high-velocity flame. Peak temperature of 2200 °C with expanding gas velocities approaching 933 m/s can be achieved based on the equivalence ratio (ratio of actual fuel to air to stoichiometric fuel to air) of

gases. Test coupons were mounted in the hydraulic grips at an angle of 45° (which we believe is the severe degrading condition a CMC can experience) and subjected to directional heating of the flame produced by HVOF gun. By adjusting the parameters of the gun, different combustion conditions are achieved (Temperature, %Water vapor, and velocity). Heating the front surface of the specimen while natural convection occurs on the back surface creates thermal gradient stresses. The expanding gases are travelling at a speed up to 933 m/s, generating excessive noise. Therefore, the experimental facility was set up in a noise-cancelling room as shown in Figure 1. To protect the hydraulic grips from heating, steel plates, and multilayer ceramic insulation sheets are used. Cold water is fed through the wedges to cool the ends of the specimen.

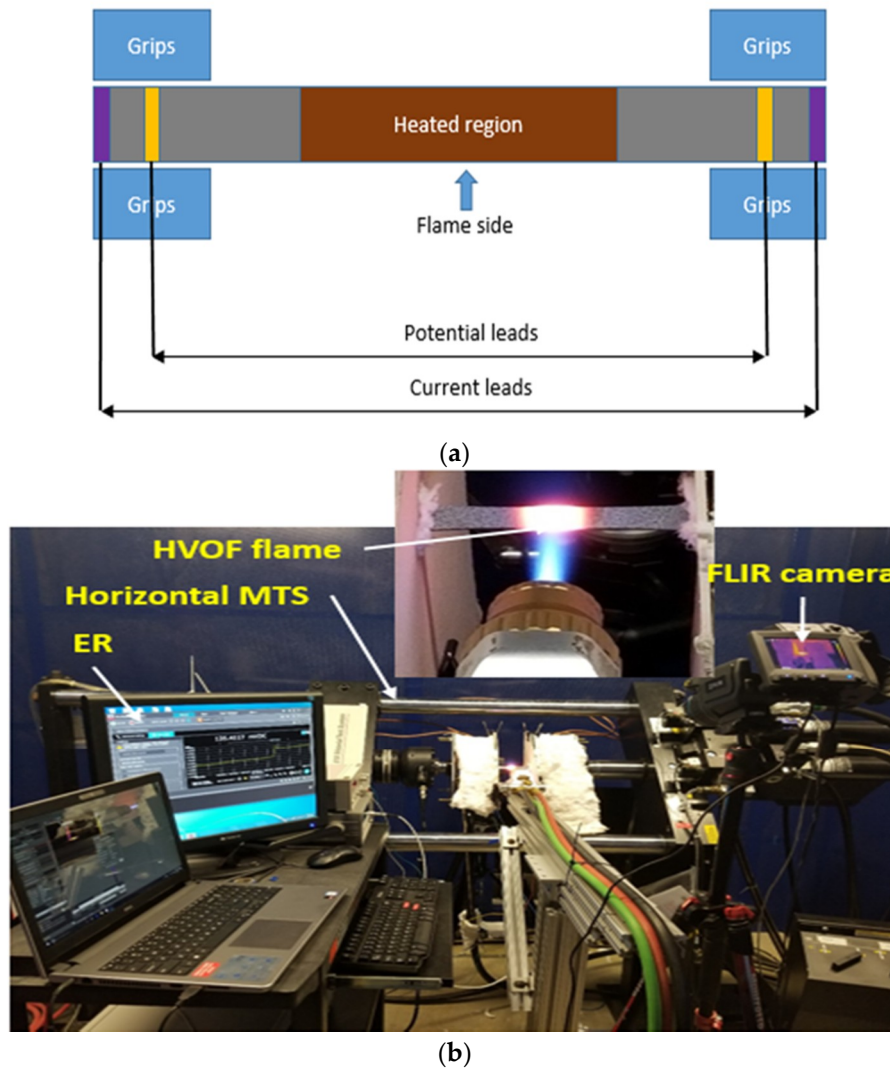


Figure 1. (a) Specimen showing electrical resistance (ER) configuration; (b) high-velocity oxygen fuel (HVOF) combustion facility setup.

Expanding gases velocity was calculated by spraying chrome carbide particles using the inlet provided on the control panel. A high-speed camera was used to record the images of the particles sprayed. Velocity was calculated by tracking the distance travelled by particles at a given time using an open source Tracker software.

Two forward lean infrared cameras (FLIR A6700 SC long wave) were used to monitor the front and back surface temperature of the specimen by inputting the known emissivity of the specimen. Emissivity was calculated using a three-inch resistance furnace with a window opening to monitor the

front surface temperature of the specimen using FLIR camera. Temperature of the furnace was raised to test temperature (measured with R-type thermocouple using AMTECO controller) alongside the surface with FLIR reading. Emissivity in the FLIR camera was adjusted until the furnace and the FLIR temperatures were matched. The apparent emissivity values of MI, CVI, and EBC-CVI specimens were 0.83, 0.91, and 0.845.

2.2. Materials Tested

A limited number of two types of 2D woven SiC/SiC composites were available for this study. Both composite types consist of eight plies of five-harness satin weave. A vintage melt-infiltrated (MI) SiC matrix composite, originally manufactured by Goodrich Corporation [18] containing Hi-Nicalon-Type S fiber-reinforcement, a CVI boron nitride (BN) interphase, and CVI silicon carbide (SiC) overcoat sub-structure prior to SiC particle infiltration and final liquid Si infiltration. The second type was manufactured using a CVI process by Rolls-Royce, (formerly Hyper-Therm High Temperature Composites in Huntington Beach, CA, USA). The CVI composites contain Hi-Nicalon fiber-reinforcement, a CVI BN interphase, and CVI SiC matrix. For some CVI composites, multilayer EBC coating was applied on the gauge section of the CVI test coupons using slurry infiltration process [19]. The EBC multilayer coating consists of mullite as a bond coat and rare earth material ytterbium monosilicate (Yb_2SiO_5) as a top coat. Slurry prepared for the first layer was primarily used to fill the pores of the CMC structure and as a bond coating. Second and third layer coating was applied using ytterbium monosilicate to fill the cracks in the primary coating and as a top coat. Once the infiltration was done, extra material was brushed off and the specimens were dried in air and sintered in air in a high-temperature furnace at 1450 °C for five hours. A coating thickness of 0.32 mm was achieved. Further details of the slurry infiltration process is provided in Zhou et al. [19].

MI specimens considered were dog bone-shaped and CVI specimens were straight-sided. All the specimens had as-machined edges, i.e., there was no seal-coat which made their exposure a worst-case scenario. Material dimensions and as-produced mechanical properties are shown in Tables 1 and 2 and microstructures are shown in Figure 2. UTS for the CVI is not shown as the specimen failed close to the top grip. Proportional limit is determined using ASTM C1275-15 based on the 0.05% strain offset method.

Table 1. Material dimensions.

Material	Length (mm)	Average Width (mm)	Average Thickness (mm)	Porosity	Test Condition
MI	152	10.74 ± 0.01	2.92 ± 0.01	-	Furnace/burner rig
CVI	152	12.74 ± 0.01	2.25 ± 0.04	10%	Furnace/burner rig
EBC-CVI	152	13.03	2.59	10%	Burner rig
EBC-CVI	152	13.09 ± 0.06	2.63 ± 0.04	18%	Furnace/burner rig

Table 2. As-produced mechanical properties.

Specimen	Ultimate Tensile Strength (UTS) MPa	Modulus (E) GPa	¹ Proportional Limit MPa
MI	263	219	123
CVI ²	-	200	110

¹ Proportional limit is established based on 0.05% strain offset stress. ² Uncoated chemical vapor infiltrated (CVI) with 10% porosity.

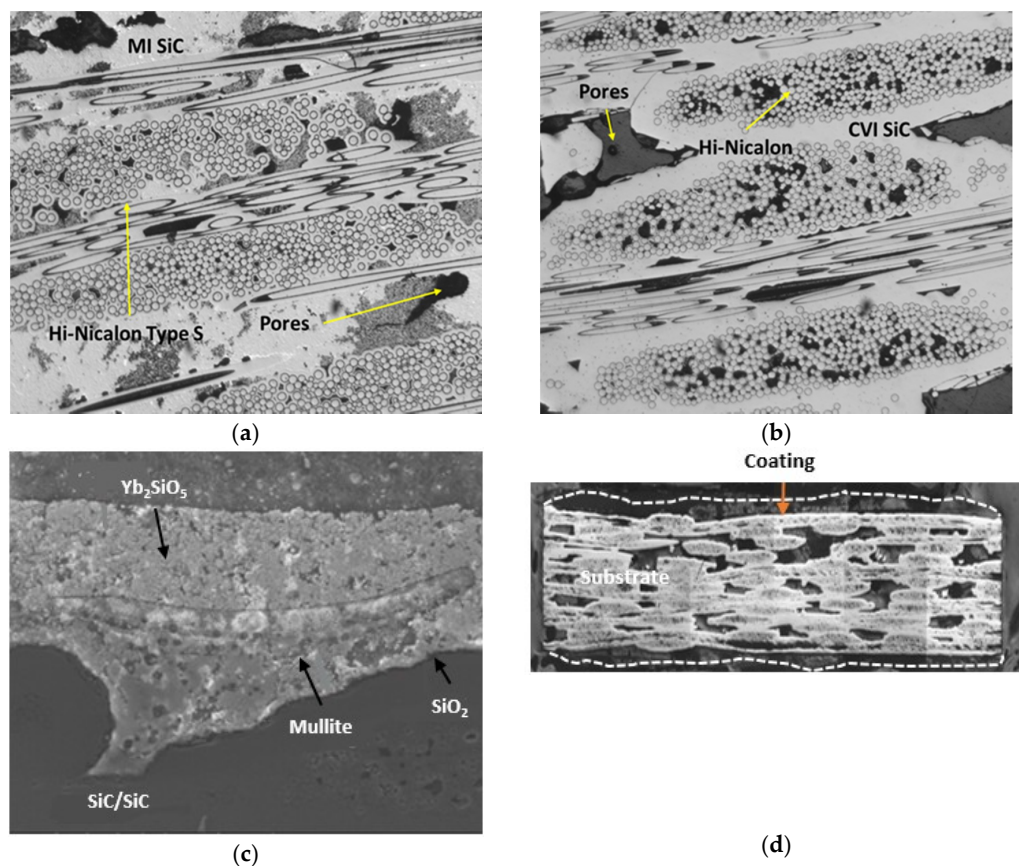


Figure 2. Microstructure of (a) melt-infiltrated (MI) Hi-Nic-S/BN/SiC, (b) CVI Hi-Nic/BN/SiC, (c) environmental barrier coating (EBC) coated CVI Hi-Nic/BN/SiC, (d) Microscope image showing coating thickness.

2.3. Burner Rig Fatigue Test

All the specimens considered for this study were subjected to a tension-tension fatigue loading at selected stress, temperature, and velocity conditions. Test parameters are specified in Table 3. Flow rates of propane, oxygen, and compressed air were adjusted to meet the specified conditions. Flow rates considered for this study were of 55 slpm (standard liters per minute) of propane, 300 slpm of oxygen and 400 slpm of compressed air with pressures of 80 psi (pounds per square inch) of propane, 150 psi of oxygen and 75 psi of compressed air. ER was incorporated as an in-situ health-monitoring technique to monitor the damage.

Table 3. Burner rig test parameters.

Parameter	Condition
Stress	100 MPa
Frequency	1 Hz
Stress ratio	0.1
Temperature	1200 °C
Specimen orientation	45°
Velocity	~650 m/s
¹ Equivalence ratio	~0.83

¹ Equivalence ratio is defined as actual fuel to air to stoichiometric fuel to air ratio.

Before loading the specimen in burner rig, the flame was started at a distance far away from the specimen to prevent the material from experiencing thermal shock. It was slowly advanced until the set target temperature was achieved while recording the surface temperature with FLIR camera. During this period, the MTS was set to maintain a minor load of 100 N to prevent the specimen going into compression due to thermal expansion from heating. The gun was kept at that position for 5 min to achieve a stable temperature distribution on the specimen surface and fatigue cycling was initiated. Initially, specimens were ramped to mean load and fatigued at 0.1 Hz for 10 cycles, 0.5 Hz for 10 cycles and 1 Hz until failure. Runout condition in the burner rig is set to a maximum duration of 24 H. If a specimen survives continuous 4 h burner rig testing (maximum per day due to safety considerations), it was dismantled from hydraulic grips and the specimen mass was measured.

2.4. Furnace Fatigue Test

To compare with a static environment, similar fatigue tests were performed with an isothermal furnace. A three-inch AMTECO resistance furnace was used with a hot zone temperature of 1200 °C during testing (25 mm hot zone length). Temperature was ramped evenly at a rate of 40 °C per minute. A maximum duration of 100 H is considered as runout condition in furnace environment.

3. Results and Discussion

3.1. Burner Rig Fatigue Test Results

Uncoated MI, CVI, and environmental barrier coating (EBC) coated CVI test coupons were tested in tension-tension fatigue loading at a peak stress of 100 MPa with combustion flame impinging on front surface. In this study fatigue life of the specimens considered is defined up to failure. Fatigue life of the test coupons tested in combustion environment is shown in Figure 3. Uncoated specimens had a shorter fatigue life compared to the EBC coated. Shorter fatigue life of the uncoated test coupons indicates the adverse effect of harsh combustion environment.

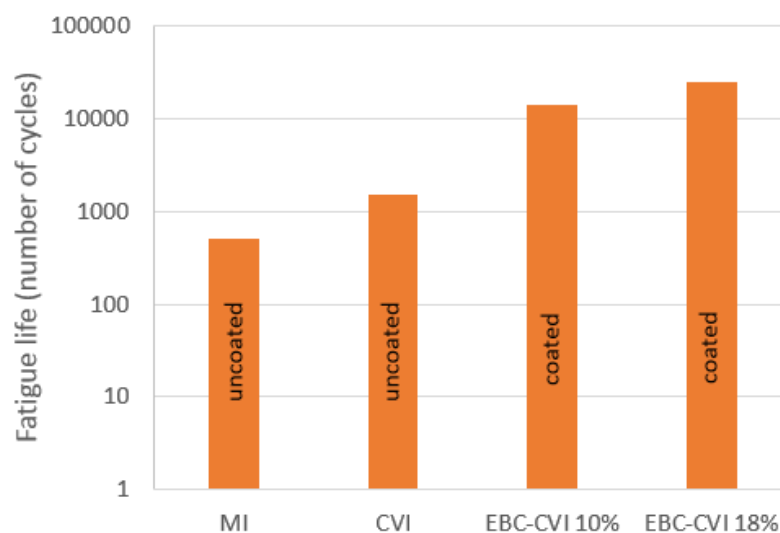


Figure 3. Fatigue life of MI, CVI, and EBC-CVI test coupons in combustion environment.

Fatigue life of 500 cycles (8 min) was observed for the MI specimen. It should be noted that the MI specimens used here were relatively weak compared to modern state-of-the-art MI composites, which could be a reason for such a low fatigue life. The uncoated CVI specimen survived 1500 cycles (25 min) while the EBC coated CVI specimens with 10% and 18% porosity content survived 14,400 cycles (240 min) and 25,200 cycles (420 min). Application of EBC coating significantly increased the fatigue life in combustion environment. Presence of voids, the exposure of as-machined edges, and the 45°

angle of incidence of the flame most likely accelerated material degradation. Comparing the two EBC coated CVI specimens, specimen with high porosity (18%) content showed a significant increase in fatigue life. This may be due to the increased infiltration of oxide into the composite. In addition, prior to testing some regions along the edges of the EBC-CVI 10% specimen were observed to not completely cover the edge exposing the as-machined edges to the environment. Also, presence of micro-cracks on the EBC coating due to slurry infiltration technique makes them more susceptible to spallation where oxidative gases can easily reach the substrate.

Temperature distribution along the length of the specimen for coated and uncoated test coupons are shown in Figure 4. Front side FLIR camera captured the entire gauge section while the back side FLIR camera captured only an inch length because of different calibration settings. A thermal gradient of 175 °C, 100 °C, and 600 °C is seen for MI, CVI, and EBC coated CVI. From the literature [1], it is observed that MI SiC/SiC has higher thermal conductivity compared to CVI SiC/SiC. However, the CVI specimens tested in this study are thinner (Table 1) than the MI specimens which would explain the lower thermal gradient for CVI.

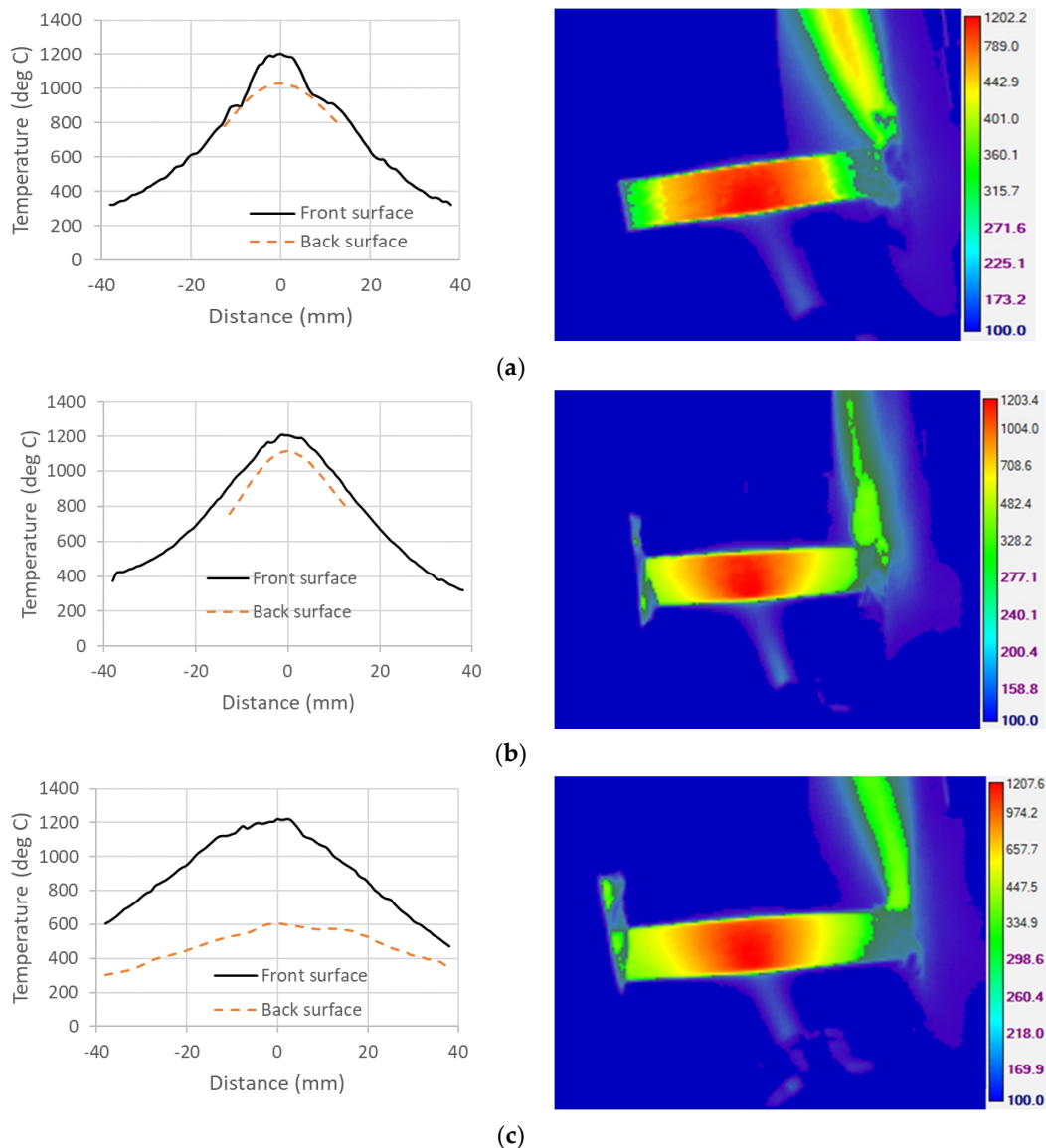


Figure 4. Temperature distribution along length from FLIR camera (front side shown) (a) MI SiC/SiC, (b) CVI SiC/SiC, (c) EBC-CVI SiC/SiC.

Resistance change with temperature for the uncoated and EBC coated test coupons are shown in Figure 5. To understand the ER behavior, the current flow path for the two material systems considered in this study has to be explained. Many researchers [17,20–22] have extensively investigated the ER behavior of MI and CVI SiC/SiC CMC systems at room temperature and high temperature under various loading conditions. MI composites are electrically more conductive compared to the CVI. In MI SiC/SiC, the matrix is the more conducting phase in comparison to the fiber. This is due to the presence of free doped silicon (Si) present in the matrix. Si is more conductive than that of the pure CVI. Morscher et al [17] estimated the resistivity of Si to be $0.046 \Omega\text{-mm}$ for iBN composite and $0.056 \Omega\text{-mm}$ for ZMI composite. Any damage to the matrix (i.e., matrix cracking) breaks the electrical network resulting in an overall increase in the resistance. The literature reported resistivity values of the CMC constituents are listed in Table 4 [17,23,24]. CVI SiC/SiC considered in this study had Hi-Nicalon fibers. From Table 4, it can be seen that resistivity of Hi-Nicalon fibers is significantly lower compared to the pure CVI SiC, and it is reasonable to assume that fibers are the majority charge carriers. Therefore, CVI SiC/SiC system is less sensitive to matrix damage compared to MI SiC/SiC.

Table 4. Electrical resistivity of ceramic matrix composites (CMC) constituents.

CMC Constituent	Electrical Resistivity ($\Omega\text{-cm}$)
CVI SiC	100–10,000 [17,23]
Si	0.0001–1000 [17,23]
Hi-Nicalon	3 [23,24]
Hi-Nicalon Type S	0.1 [23]

The high-temperature ER response of the MI SiC/SiC system is significantly different compared to the CVI SiC/SiC due to the presence of silicon enriched matrix. Resistance of Si increases with temperature, whereas the resistance of SiC decreases with temperature. Similar ER behavior, as discussed above, is observed in the burner rig for MI and CVI SiC/SiC composites, respectively (Figure 5). MI composite resistance significantly increased with heating and upon loading a more gradual increase in resistance was observed until failure (Figure 5a). CVI composite resistance significantly decreased with heating and an increase in resistance is seen with loading (Figure 5b–d). This gradual increase in resistance could be attributed to fatigue loading and possible oxidative degradation [25].

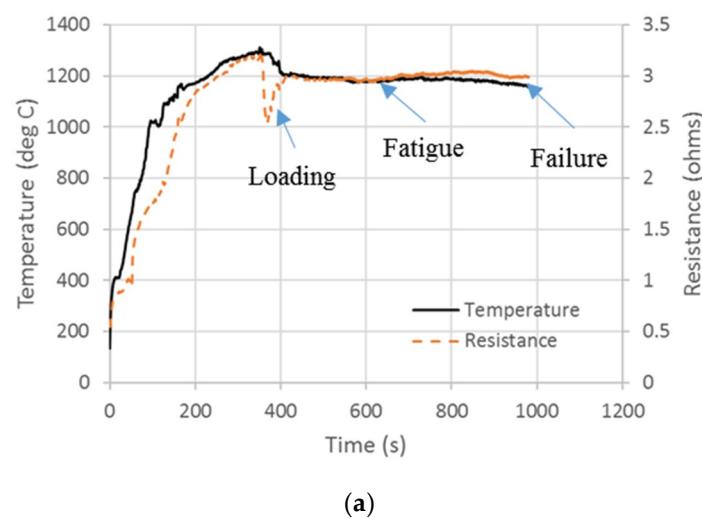


Figure 5. Cont.

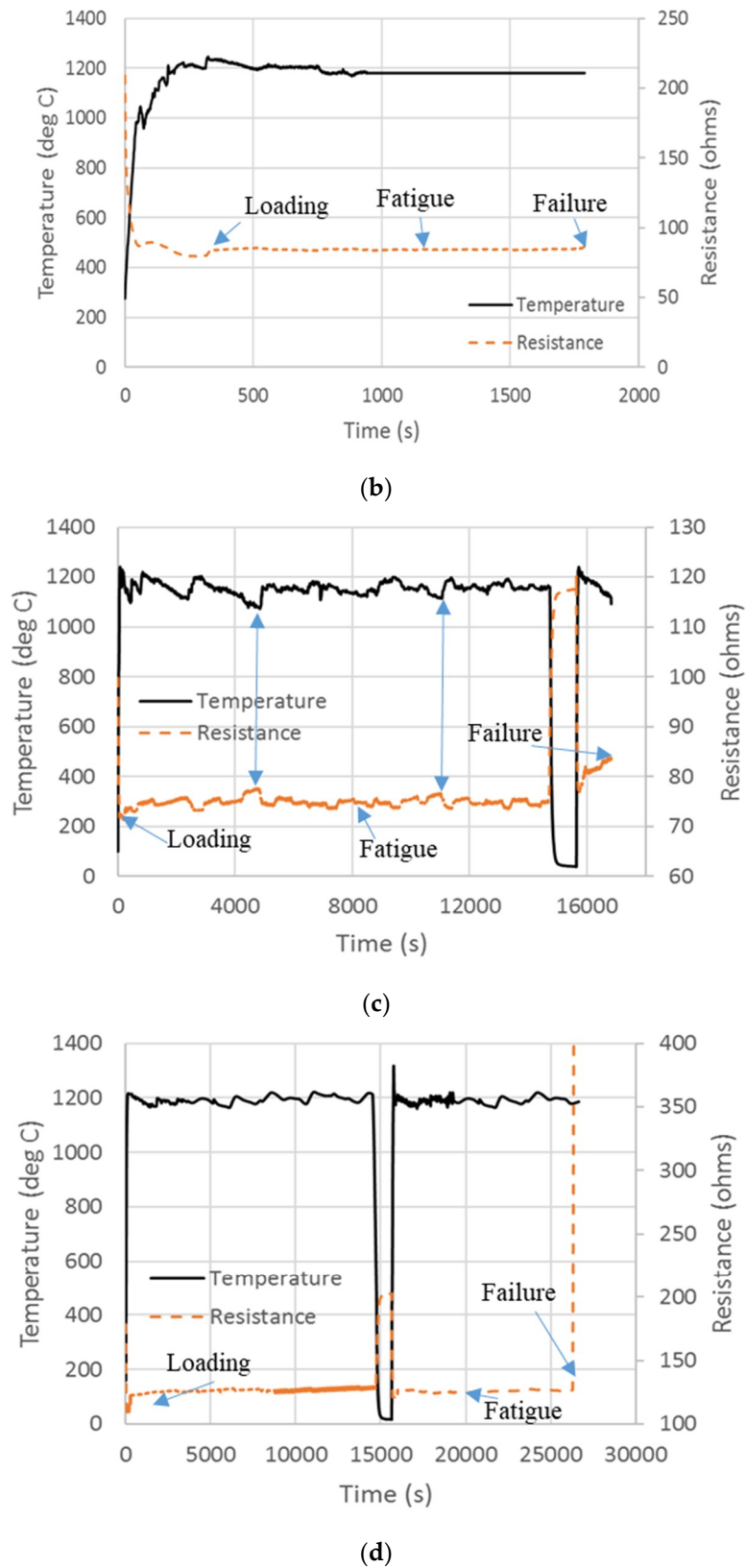


Figure 5. ER profile with temperature in combustion environment (a) MI SiC/SiC, (b) CVI SiC/SiC, (c) EBC-CVI 10%, (d) EBC-CVI 18%.

For one of the EBC coated CVI SiC specimens (Figure 5c), there were intermittent increases and decreases in resistance during burner rig fatigue. The increases corresponded with temperature decreases and the decreases with temperature increases, showing the sensitivity of resistance to temperature fluctuations possible due to open-flame heating. The resistance of the specimens before, during, and just prior to failure in burner rig is shown in Table 5. Some measurements were made at room temperature (RT) and others at temperature. An increase in resistance was observed for all the CVI specimens at temperature and the CVI-EBC specimens after 4 h of testing when measured at room temperature. This residual or irreversible resistance is presumed to be due to nonrecoverable damage to the fibers and matrix. The MI specimen actually showed a little net increase in resistance at temperature. However, this was probably due to the apparent gradual reduction in temperature during the test (Figure 5a).

Table 5. Resistance change in burner rig.

Specimen	Room Temperature (RT) ER (Ω)	Resistivity (Ω -mm)	ER @ 1200 °C before Loading (Ω)	RT ER after 4H (Ω)	ER before Failure @ 1200 °C (Ω)
MI	0.524	0.16	2.9	-	3.0
CVI	208	61.8	84	-	92
CVI-EBC 10%	114	34.1	74	121	83
CVI-EBC 18%	179	55.5	125	199	130

3.2. Furnace Testing

To compare to the combustion test results, test coupons were tested in isothermal furnace at a peak temperature (1200 °C), the same as the surface temperature of the combustion test. Fatigue life of the uncoated and coated specimens is shown in Figure 6. The fatigue life for MI was 6.5 h (23,400 cycles); for CVI as-produced, it was 100 h (360,000 cycles); and for the EBC coated CVI, it was 4 h (14,400 cycles). Furnace tested specimens showed a significant increase in fatigue life compared to the combustion tested uncoated specimens. Higher fatigue life observed in the furnace could be due to the absence of water vapor and thermal gradient stresses. Higher fatigue life seen for the EBC-CVI 18% porosity specimen in burner rig compared to furnace tested specimen could be due to increased infiltration of oxide into the composite. The significance of thermal gradient stress and watervapor on fatigue life is discussed in detail in the "General discussion" section.

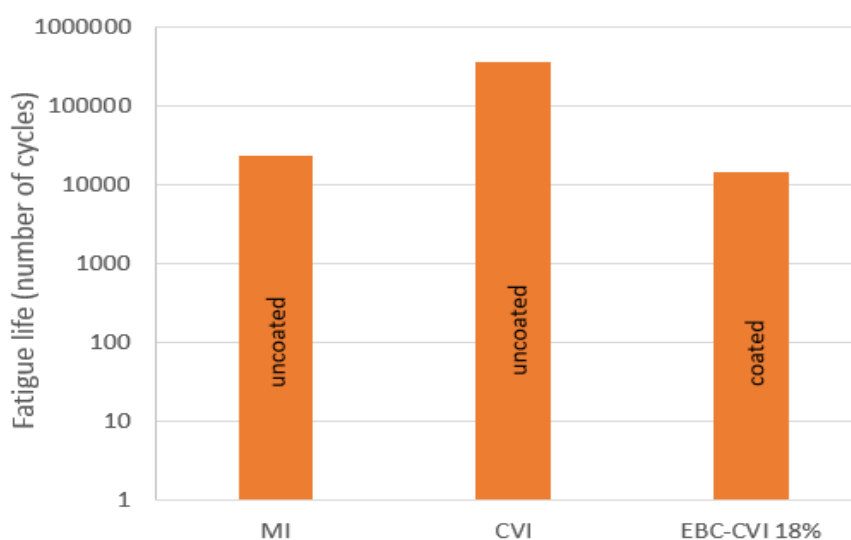


Figure 6. Fatigue life of uncoated and coated test coupons in isothermal furnace.

Surprisingly, the uncoated CVI significantly outperformed the EBC coated CVI for the furnace fatigue condition. EBC coating processing required sintering at 1450 °C for several hours. Heat-treating the composite for such a long duration exposes the Hi-Nicalon fibers to temperatures well above their processing temperature and is known to degrade the fiber strength by 60% [26–29]. This suggests that application of EBC coating using slurry infiltration technique provides the oxidation resistance but significantly reduces the fiber strength for this composite system due to thermal exposure during coating processing. However, if Hi-Nicalon S fibers were used in the CVI SiC system, such degradation would not be expected.

ER profiles with temperature for the MI, CVI, and EBC coated CVI specimens are shown in Figure 7. For the MI specimen, resistance increased with heating up to 950 °C and beyond this resistance decreased. Smith et al [23] reported that resistivity of silicon varies with dopant level and there is a saturation temperature where the resistance increases with time (below the saturation temperature) and above saturation temperature resistance decreases. The increase in resistance below the saturation temperature is attributed to the precipitation of dopants from the silicon and the decrease above saturation temperature is attributed to the increase in carrier concentration due to reabsorption of dopants.

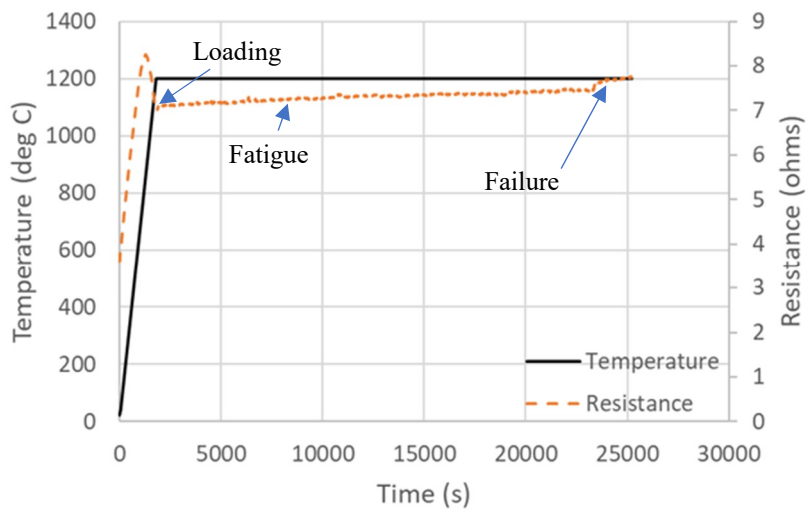
This behavior is not seen in the burner rig MI specimens, which we believe to be due to difference in the temperature distribution along the length of the specimen. The three-inch furnace and the burner rig both have a hot zone (1200 °C) of approximately 25 mm (Figure 4). However, the furnace temperature both within and outside the hot zone is uniform across the cross-section of the composite and the axial temperature gradient is relatively stable. The burner rig has a temperature gradient through the thickness of the specimen so that the hottest region of the specimen is at the surface of the flame side. The resistivity of the regions outside the flame-side surface are higher for temperatures from ~900 to 1200 °C. These high resistances presumably would mask the decrease in resistance experienced in the hot zone above the saturation temperature, resulting in a continuous increase in resistance. With loading, an increase in resistance is seen, and finally, failure where resistance changes is abrupt. Observed ER trend for CVI and EBC coated CVI composite in furnace is similar to the burner rig where the resistance decreased with heating and with loading resistance increased until failure.

ER change in furnace tested specimens is shown in Table 6. Uncoated CVI specimen showed no change in ER after 100 h of testing, which implies that the applied stress did not cause any significant matrix cracking to the composite. The smooth ER trend in the furnace is due to uniform increase of temperature.

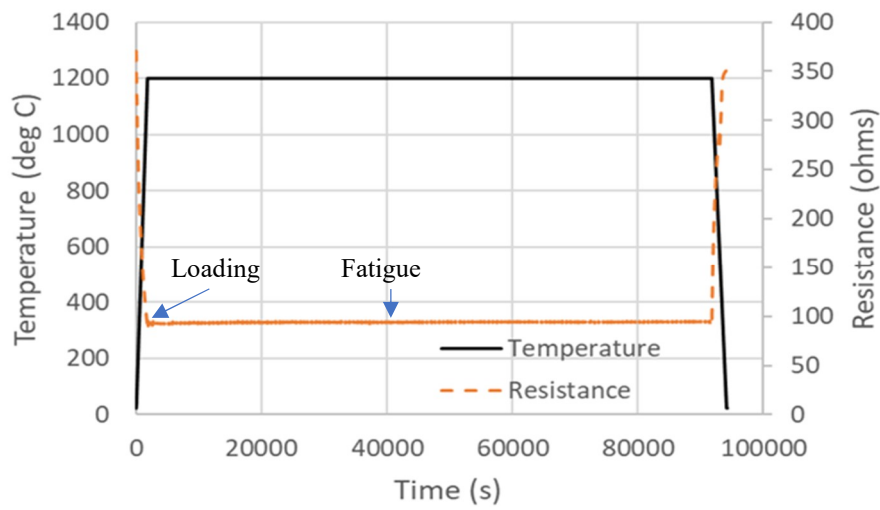
Table 6. Resistance change in furnace.

Specimen	RT ER (Ω)	Resistivity (Ω-mm)	ER @ 1200 °C before Loading (Ω)	ER before Failure @ 1200 °C
MI	3.6	1.07	7.1	7.77
CVI	370	79.99	92	*NA
EBC-CVI 18%	165	47.41	55	58

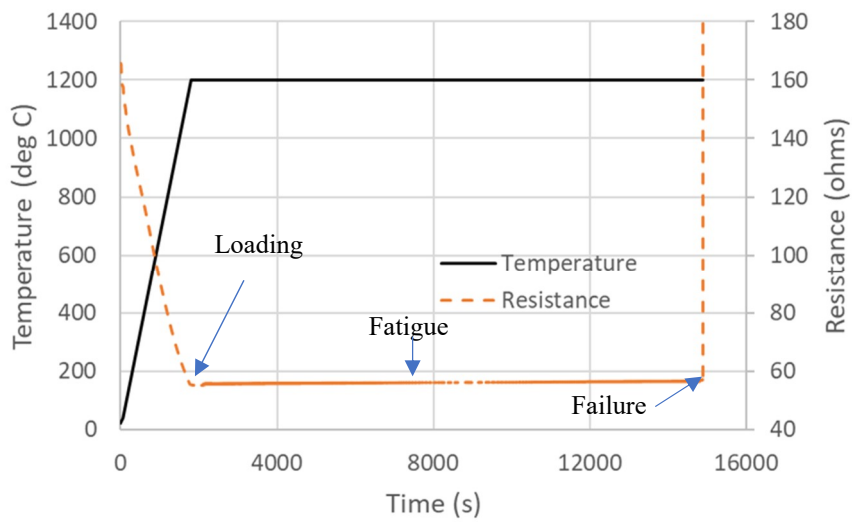
* Runout specimen, no change in ER at RT after 100 h fatigue at temperature exposure.



(a)



(b)



(c)

Figure 7. ER trend with temperature in isothermal furnace (a) MI SiC/SiC and (b) CVI SiC/SiC for first 25 h of testing (c) EBC-CVI 18%.

3.3. Microscopic Analysis

Fracture surfaces of the failed test coupons were observed under SEM to understand the damage mechanisms and the extent of oxidation. Microscopy images of fracture surfaces of MI, CVI, and EBC coated CVI test coupons tested under combustion and furnace conditions are shown in Figure 8.

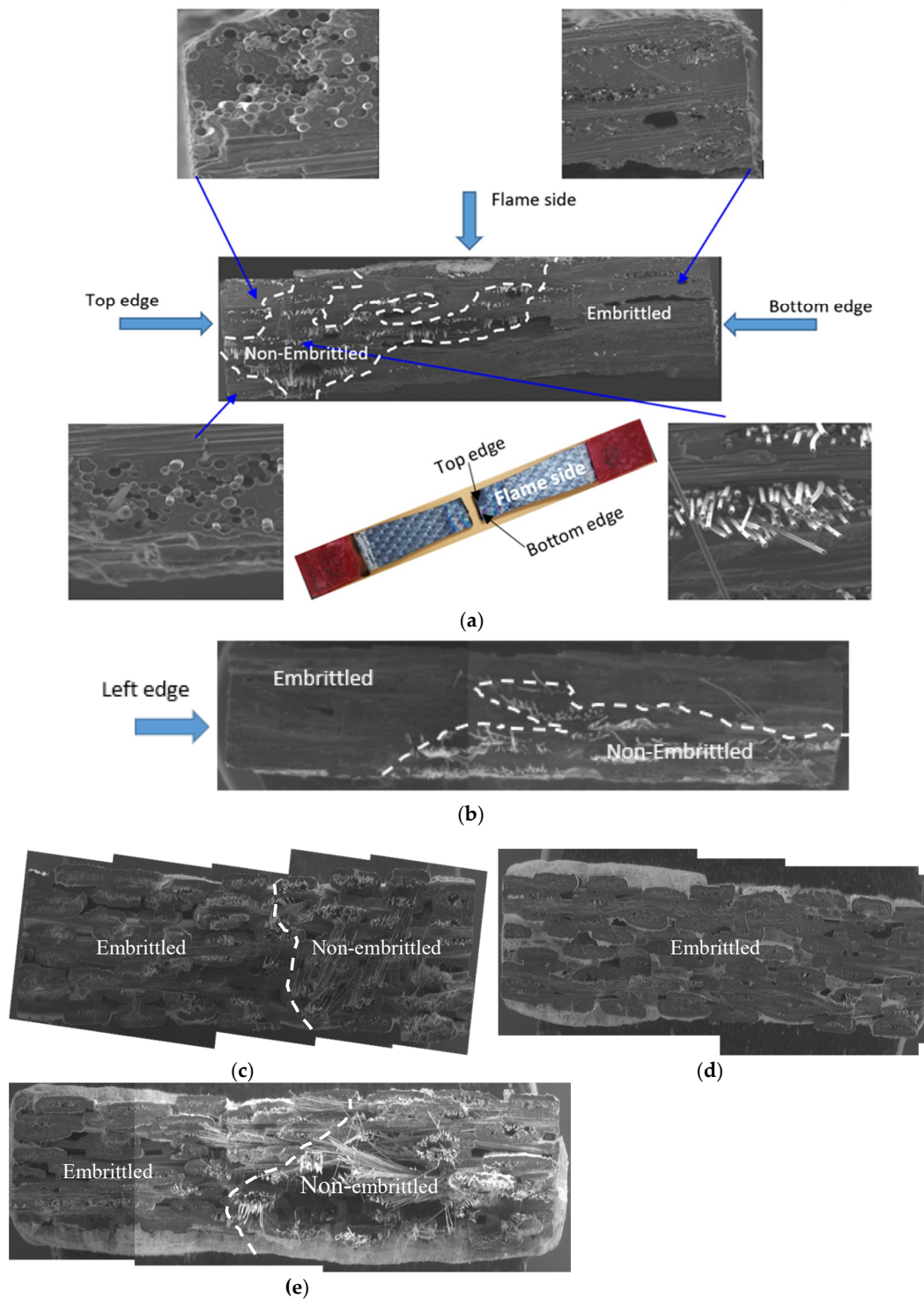


Figure 8. Microscopic images of fracture surface (a) MI combustion test, (b) MI furnace test, (c) CVI combustion test, (d) EBC coated CVI combustion test, (e) EBC coated CVI furnace test.

From SEM images, it is clearly evident that majority regions of the fracture surface of the test coupons tested in combustion facility (Figure 8a,c) are oxidized with little fiber pullout. Oxidized regions are indicated as embrittled and unoxidized/fiber pullout regions are indicated as non-embrittled. The two regions are separated by a white dotted line. In oxidized regions, matrix and the BN interphase are completely oxidized, and the fibers are fused together by the oxides, whereas no signs of oxidation are seen on the fibers in the pullout area. Burner rig test coupons suffered significant oxidation, which could be attributed to the hostile environment with harsh combustion gases. Edges of the test coupons (Figure 8a) tested in combustion environment are completely oxidized clearly indicating an edge effect. Edge effect is predominantly seen in burner rig due to angular impingement (45°) of flame on test coupons. As a result, top and bottom edges of the specimen were completely exposed to high temperature high velocity flame. It appears that loading initiated micro-cracks, which serve as a free path for the high-temperature gases to enter the composite system, causing embrittlement and finally a dominant crack is originated from the edges. Figure 9 shows the FLIR image of the CVI test coupon near failure in burner rig indicating the failure from the bottom edge. This is consistent with the fracture surface (Figure 8a) where the embrittled region extends more deeply from the bottom edge (nearest to nozzle) than the top edge.

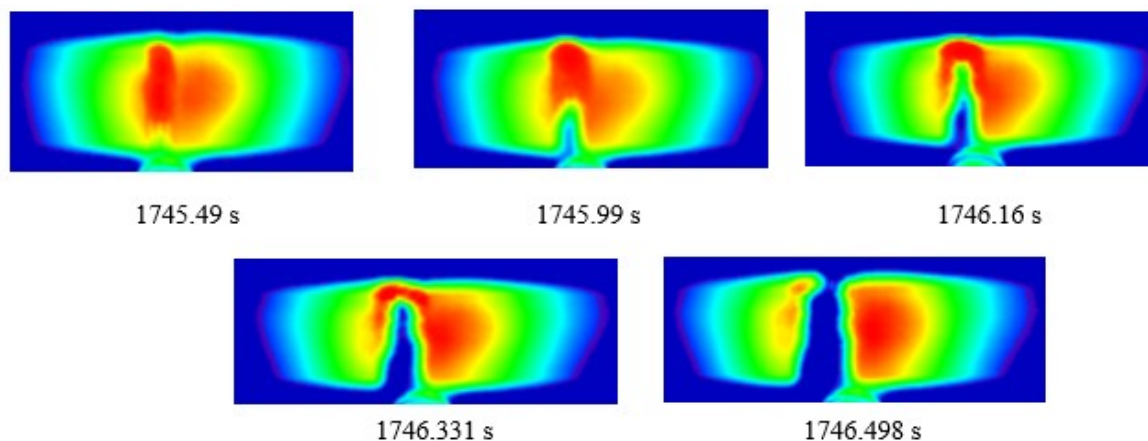


Figure 9. Backside FLIR images of CVI specimen in combustion environment showing failure originating from the edge.

Fracture surface of the EBC coated CVI specimens (Figure 8d) showed a planar fracture with no fiber pullout and complete oxidation of BN interphase. Application of EBC coating increased the fatigue life of the specimen. However, coating spallation, which leads to the exposure of the as-machined edges, formation of micro-cracks due to loading, and longer time for the cracks to propagate, made the hot combustion gases diffuse through the cracks leading to complete oxidation of fibers and matrix.

For the furnace tested specimen, oxidation likely appeared to be originated from the left edge (Figure 8b,e) and a little fiber pullout is seen on the other edge. In the oxidized areas, BN interphase is completely oxidized, causing fibers to bond together, whereas no oxidation is seen on fibers in non-embrittled areas. Fracture surface reveals that cracks are initiated from the machined edges. As the crack grows, more regions are exposed to oxidative environment, causing embrittlement. Presumably embrittled areas transfer the load to remaining intact areas, which are incapable of carrying the load leading to final failure [30,31].

4. General Discussion

Fatigue lives observed for uncoated and coated specimens at the same applied stress level are longer when tested in the furnace than in the combustion facility. Fixing the specimen ends and directional heating of the specimen front surface induces thermal stress. An approximate estimate of

the induced thermal stress and temperature distribution along the through-thickness direction for the uncoated specimens is shown in Figure 10. Through-thickness temperature distribution is calculated using simplified 1D steady state heat transfer approximation and thermal stress is calculated based on the simplified equation deduced by Appleby [32] as shown in Equation (1).

$$\sigma_t = -\alpha E \left(\frac{T_{front} - T_{back}}{t} \times z + \frac{T_{front} + T_{back}}{2} \right) + \frac{1}{2} \alpha E (T_{front} + T_{back}) \quad (1)$$

where α is coefficient of thermal expansion, E is elastic modulus, t is thickness, T_{front} is front surface temperature, T_{back} is back surface temperature, and Z is through thickness distance where thermal stress is measured.

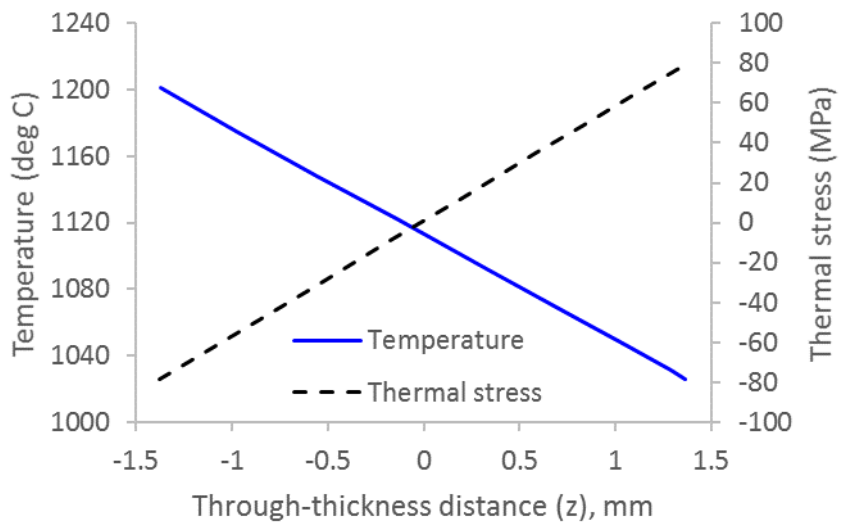
Elastic modulus and coefficient of thermal expansion are taken from the literature [33,34] and front and back surface temperatures are taken from FLIR. High velocity of the flame induces compressive stress on the front surface of the specimen while back surface experiences tensile stress. A net thermal stress increase/decrease of 79 MPa is estimated for the back/front sides of the MI specimen and a net increase/decrease of 50 MPa is estimated for the back/front of the CVI specimen. Addition of the thermal stress to the applied stress (back side) would be expected to induce increased matrix cracking and accelerated material degradation leading to embrittlement and failure. Note that the oxidation embrittlement was more pronounced on the back side of the burner rig tested MI and CVI specimens, Figure 8a,c, respectively. It should be noted that thermal stress estimated here is an approximation based on steady state assumptions and simplified Equation (1). However, these results indicate that thermal stress has a deleterious effect in burner rig environment, and significantly reduces fatigue life when combined with water vapor.

Coated specimen of same porosity (10%) content showed an increased fatigue life than the uncoated specimen shown in Figure 3, indicating EBC coatings are beneficial for SiC/SiC CMCs to survive in combustion environments. Although coatings significantly increase the fatigue life, spallation is a serious issue in burner rig environment. Figure 11 shows the images of EBC-CVI 18% test coupon after 4 h of testing and at failure in combustion facility. Mass of the test coupon is 11.27 g prior to testing and after 4 h of testing a reduction in weight by 0.27 g is seen due to coating spallation. A significant amount of spallation is seen after 7 h of testing on the surface. As mentioned earlier, these coatings have micro-cracks due to slurry infiltration and susceptibility in high-velocity flame to spallation, exposing the as-machined edges. Failure initiated from the bottom edge of the test coupon where coating started to spall as shown in Figure 11.

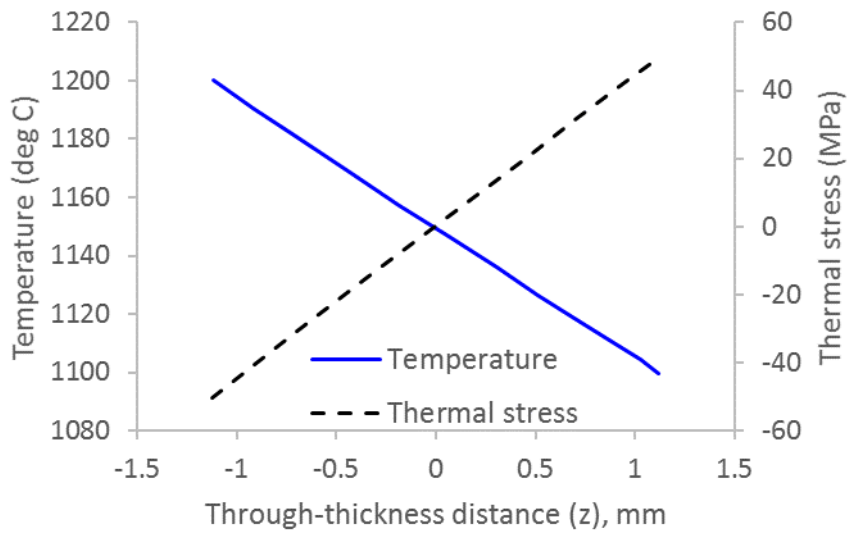
Rapid failure of the specimens in burner rig (500 and 1500 cycles for uncoated MI and CVI) suggests that velocity might be another major factor, along with water vapor and thermal stress, which significantly affects the life of the component. Ruggles-Wren et al. [29] showed fatigue life of several thousand cycles for similar Hi-NiC/BN/CVI SiC specimens in near 100% steam environment. This suggests that moisture content is not a sole factor for such a short fatigue life in burner rig. Moisture content in the burner rig is estimated to be approximately 30% by NASA chemical equilibrium analysis (NASA CEA) [35] software. Expanding gases are travelling at a speed of ~650 m/s (Table 4). This high velocity would have pushed the oxidizing gases deep into the core of the composite accelerating the volatilization of SiO₂ resulting in rapid recession of material. Opila et al. [36] showed that recession rate of the material depends on the velocity of the oxidizing gases as shown in Equation (2).

$$k_1 = \frac{v^{1/2} P(H_2O)^2}{P_{total}^{1/2}} \quad (2)$$

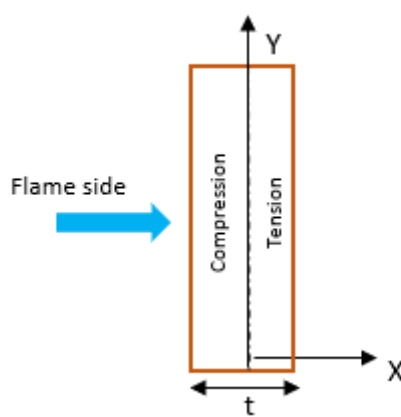
where k_1 is recession rate, v is velocity of the flame, P_{H_2O} is the partial pressure of water vapor, and P_{total} is the total pressure. From Equation (2), it is observed that recession rate is proportional to $v^{1/2}$. As a result, it is reasonable to assume that velocity plays a significant role on the life of the composites in the burner rig.



(a)



(b)



(c)

Figure 10. Through thickness thermal stress and temperature (a) MI SiC/SiC, (b) CVI SiC/SiC, (c) test coupon showing tension and compression planes in burner rig.

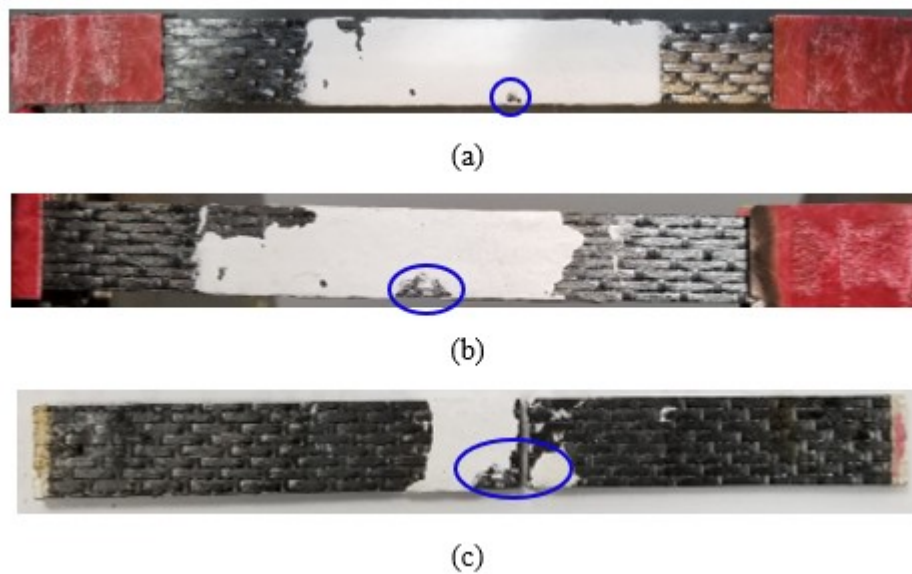


Figure 11. EBC-CVI 18% test coupon showing spallation after (a) 4 h of testing, (b) 7 h of testing, and (c) at failure.

5. Conclusions

Uncoated MI Hi-NiC-S/BN/SiC and CVI Hi-NiC/BN/SiC and ytterbium monosilicate EBC coated CVI Hi-NiC/BN/SiC test coupons were tested under fatigue loading in a combustion facility capable of simulating combustion environment and in an isothermal furnace. All the test coupons were subjected to similar test conditions. Fatigue life was greater in a static furnace environment than in the high-velocity combustion environment at the same maximum temperature condition and applied stress level for all composite/coating types, indicating the detrimental effect of the combustion environment. Microstructural observations revealed that oxidative embrittlement is more in burner rig environment compared to the furnace environment. Further, oxidized edges of the burner rig specimens reveal the serious effect of 45° angle of incidence of the flame.

Application of slurry infiltrated EBC coating significantly increased the fatigue life in burner rig environment. However, prolonged exposure to the high-velocity flame caused a significant coating spallation where failure initiated from the spallated area.

Thermal gradient stress analysis on the burner rig specimens was performed using 1D steady state heat transfer approximations. The results indicate that addition of thermal gradient stress to the applied stress could locally elevate the overall stress state and can cause significant damage reducing the fatigue life. All of this demonstrates the complicated factors that contribute to high temperature, extreme environment degradation of ceramic matrix composites, which must be accounted for when desiring to use these composites in different stressed-oxidative conditions.

Electrical resistance was implemented to monitor the composites in the combustion facility. It was observed that ER is very sensitive to temperature distribution and variation. Most tests showed gradual increase in ER during fatigue cycling, presumably due to damage development (fatigue loading and/or oxidation).

Author Contributions: R.P.P., under the guidance of G.N.M., performed the experiments and analyzed the data presented in this paper. K.M. and M.J.P. helped with the experiments. J.Z. under the supervision of G.G.C. infiltrated the ebc coatings on the CVI specimens.

Funding: This research was funded by ONR under research grant number N00014-14-1-0433, managed by David Shiffler.

Conflicts of Interest: The authors declare no conflict of interest.

References

1. Brewer, D. HSR/EPM combustor materials development program. *Mater. Sci. Eng. A* **1999**, *261*, 284–291. [[CrossRef](#)]
2. Lee, K.N.; Fox, D.S.; Bansal, N.P. Rare earth silicate environmental barrier coatings for SiC/SiC composites and Si₃N₄ ceramics. *J. Eur. Ceram. Soc.* **2005**, *25*, 1705–1715. [[CrossRef](#)]
3. Bhatt, R.T.; Choi, S.R.; Cosgriff, L.M.; Fox, D.S.; Lee, K.N. Impact resistance of uncoated SiC/SiC composites. *Mater. Sci. Eng. A* **2008**, *476*, 20–28. [[CrossRef](#)]
4. Opila, E.J.; Verrilli, M.J.; Robinson, R.C. Borosilicate Glass-Induced Fiber Degradation of SiC/BN/SiC Composites Exposed in Combustion Environments. *Int. J. Appl. Ceram. Technol.* **2016**, *13*, 434–442. [[CrossRef](#)]
5. Zhu, D.; Choi, S.R.; Eldridge, J.I.; Lee, K.N.; Miller, R.A. *Surface Cracking and Interface Reaction Associated Delamination Failure of Thermal and Environmental Barrier Coatings*; NASA Technical Report; NASA: Washington, DC, USA, 2013.
6. Lee, K.N. Key Durability Issues with Mullite-Based Environmental Barrier Coatings for Si-Based Ceramics. *Gas Turbine Power* **2000**, *122*, 632–636. [[CrossRef](#)]
7. Zhu, D.; Lee, K.N.; Miller, R.A. Thermal gradient cyclic behavior of a thermal/environmental barrier coating system on sic/sic ceramic matrix composites. In Proceedings of the ASME Turbo Expo 2002: Power for Land, Sea, and Air, Amsterdam, The Netherlands, 3–6 June 2002.
8. Morscher, G.N. Tensile creep and rupture of 2D-woven SiC/SiC composites for high temperature applications. *J. Eur. Ceram. Soc.* **2010**, *30*, 2209–2221. [[CrossRef](#)]
9. Morscher, G.N.; Ojard, G.; Miller, R.; Gowayed, Y.; Santhosh, U.; Ahmed, J.; John, R. Tensile creep and fatigue of Sylramic-iBN melt-infiltrated SiC matrix composites: Retained properties, damage development, and failure mechanisms. *Compos. Sci. Technol.* **2008**, *16*, 3305–3313. [[CrossRef](#)]
10. Ruggles-Wrenn, M.B.; Christensen, D.T.; Chamberlain, A.L.; Lane, J.E.; Cook, T.S. Effect of frequency and environment on fatigue behavior of a CVI SiC/SiC ceramic matrix composite at 1200 °C. *Compos. Sci. Technol.* **2011**, *71*, 190–196. [[CrossRef](#)]
11. Kim, T.T.; Mall, S.; Zawada, L.P. Fatigue characterization of a melt infiltrated woven Hi-NiC-S/BN/SiC ceramic matrix composite using a unique combustion facility. *Ceram. Trans.* **2009**, *179*, 103–116.
12. Kim, T.T.; Mall, S.; Zawada, L.P.; Jefferson, G. Simultaneous fatigue and combustion exposure of SiC/SiC ceramic matrix composite. *J. Compos. Mater.* **2011**, *44*, 2991–3016. [[CrossRef](#)]
13. Sabelkin, V.; Mall, S.; Cook, T.S.; Fish, J. Fatigue and creep behaviors of a SiC/SiC composite under combustion and laboratory environments. *J. Compos. Mater.* **2016**, *50*, 2145–2153. [[CrossRef](#)]
14. Linus, U.J.T.O. A pervasive mode of oxidative degradation in a SiC-SiC composite. *J. Am. Ceram. Soc.* **1999**, *81*, 2777–2784.
15. Appleby, M.P.; Zhu, D.; Morscher, G.N. Mechanical properties and real-time damage evaluations of environmental barrier coated SiC/SiC CMCs subjected to tensile loading under thermal gradients. *Surf. Coat. Technol.* **2015**, *284*, 318–326. [[CrossRef](#)]
16. Smith, C.E.; Morscher, G.N.; Xia, Z. Electrical resistance as a nondestructive Evaluation Technique for SiC/SiC Ceramic Matrix Composites under Creep-Rupture Loading. *Int. J. Appl. Ceram. Technol.* **2011**, *8*, 298–307. [[CrossRef](#)]
17. Morscher, G.N.; Baker, C.; Smith, C. Electrical Resistance of SiC Fiber Reinforced SiC/SiC Matrix Composites at Room Temperature during Tensile Testing. *Int. J. Appl. Ceram. Technol.* **2014**, *11*, 263–272. [[CrossRef](#)]
18. Morscher, G.N.; Pujar, V.V. Melt-Infiltrated SiC composites for gas turbine engine applications. In Proceedings of the ASME Turbo Expo Land, Sea and Air 2004, Vienna, Austria, 14–17 June 2004.
19. Zhou, J.; Chase, G.G.; Almansour, A.; Morscher, G.N.; Harder, B.; Fox, D. EBC Slurry Infiltrated Matrix/Coatings for Woven SiC/SiC Composites. *Ceram. Eng. Sci. Proc.* **2018**, *38*, 137–145.
20. Smith, C.E. Monitoring Damage Accumulation in SiC/SiC Ceramic Matrix Composites Using Electrical Resistance. Master's Thesis, The University of Akron, Akron, OH, USA, 2009.
21. Smith, C.E.; Morscher, G.N.; Xia, Z.H. Monitoring damage accumulation in ceramic matrix composites using electrical resistivity. *Scr. Mater.* **2008**, *59*, 463–466. [[CrossRef](#)]
22. Morscher, G.N.; Smith, C.E.; Maillet, E.; Baker, C.; Mansour, R. Electrical resistance monitoring of damage and crack growth in advanced SiC-based ceramic composites. *Am. Ceram. Soc. Bull.* **2014**, *93*, 28–31.

23. Smith, C.E. Electrical Resistance Changes of Melt Infiltrated SiC/SiC Subject to Long-Term Tensile Loading at Elevated Temperatures. Ph.D. Thesis, The University of Akron, Akron, OH, USA, 2016.
24. Available online: <http://www.coiceramics.com/nicalonfiber.html> (accessed on 9 June 2019).
25. Smith, C.E.; Xia, Z.; Morscher, G.N. *Electrical Resistance of SiC/SiC Ceramic Matrix Composites for Damage Detection and Life-Prediction*; BiblioGov: Washington, DC, USA, 2019.
26. Yun, H.M.; DiCarlo, J.A.; Ogbuji, L.T.; Chen, Y.L. Tensile Behavior of As-Fabricated and Burner Rig Exposed SiC/SiC Composites with Hi-Nicalon Type-S Fibers. *Ceram. Eng. Sci. Proc.* **2002**, *23*. [[CrossRef](#)]
27. Takeda, M.; Urano, A.; Sakamoto, J.; Imai, Y. Microstructure and oxidative degradation behavior of silicon carbide fiber Hi-Nicalon type S. *J. Nucl. Mater.* **1998**, *258*, 1594–1599. [[CrossRef](#)]
28. Yun, H.M.; Goldsby, J.C.; DiCarlo, J.A. Effects of Thermal Treatment on Tensile Creep and Stress-Rupture Behavior of Hi-Nicalon SiC Fibers. *Ceram. Eng. Sci. Proc.* **2008**, *16*, 987–996.
29. Yun, H.M.; DiCarlo, J.A. Thermomechanical Behavior of Advanced SiC Fiber Multifilament Tows. In Proceedings of the 20th Annual Conference on Composites, Advanced Ceramics, Materials, and Structures, Cocoa Beach, FL, USA, 7–11 January 1996.
30. Ruggles-Wrenn, M.; Boucher, N.; Przybyla, C. Fatigue of three advanced SiC/SiC ceramic matrix composites at 1200 °C in air and in steam. *Int. J. Appl. Ceram. Technol.* **2017**, *15*, 3–15. [[CrossRef](#)]
31. Morscher, G.N.; Hurst, J.; Brewer, D. Intermediate-temperature stress rupture of a woven Hi-Nicalon, BN-interphase, SiC-matrix composite in air. *J. Am. Ceram. Soc.* **2000**, *83*, 1441–1449. [[CrossRef](#)]
32. Appleby. High Temperature Damage Characterization of Ceramic Composites and Protective Coatings. Ph.D. Thesis, The University of Akron, Akron, OH, USA, 2016.
33. Corman, G.S.; Luthra, K.L. Silicon melt-infiltrated ceramic composites (HiPerComp). In *Handbook of Ceramics Composites*; Bansal, N.P., Ed.; Kluwer Academic: New York, NY, USA, 2005; pp. 99–115.
34. Lamon, J. Chemical Vapor Infiltrated SiC/SiC composites (CVI SiC/SiC). In *Handbook of Ceramics Composites*; Bansal, N.P., Ed.; Kluwer Academic: New York, NY, USA, 2005; pp. 55–76.
35. Available online: <https://www.grc.nasa.gov/www/CEAWeb/> (accessed on 9 June 2019).
36. Opila, E.J.; Hann, R.E., Jr. Paralinear oxidation of CVD SiC in watervapor. *J. Am. Ceram. Soc.* **1997**, *80*, 197–205. [[CrossRef](#)]



© 2019 by the authors. Licensee MDPI, Basel, Switzerland. This article is an open access article distributed under the terms and conditions of the Creative Commons Attribution (CC BY) license (<http://creativecommons.org/licenses/by/4.0/>).